

Multivariate Non–Normality in WMAP 1st Year Data

Patrick Dineen^{1,2*} & Peter Coles²

¹*Astrophysics Group, Blackett Laboratory, Imperial College, Prince Consort Road, London SW7 2AZ, United Kingdom*

²*School of Physics & Astronomy, University of Nottingham, University Park, Nottingham, NG7 2RD, United Kingdom*

5 February 2008

ABSTRACT

The extraction of cosmological parameters from microwave background observations relies on specific assumptions about the statistical properties of the data, in particular that the p -point distributions of temperature fluctuations are jointly-normal. Using a battery of statistical tests, we assess the multivariate Gaussian nature of the Wilkinson Microwave Anisotropy Probe (WMAP) 1st year data. The statistics we use fall into three classes which test different aspects of joint-normality: the first set assess the normality of marginal (one-point) distributions using familiar univariate methods; the second involves statistics that directly assess joint-normality; and the third explores the evidence of non-linearity in the relationship between variates. We applied these tests to frequency maps, ‘foreground-cleaned’ assembly maps and all-sky CMB-only maps. The assembly maps are of particular interest as when combined with the kp2 mask, we recreate the region used in the computation of the angular power spectrum. Significant departures from normality were found in all the maps. In particular, the kurtosis coefficient, D’Agostino’s statistic and bivariate kurtosis calculated from temperature pairs extracted from all the assembly maps were found to be non-normal at 99% confidence level. We found that the results were unaffected by the size of the Galactic cut and were evident on either hemisphere of the CMB sky. The latter suggests that the non-Gaussianity is not simply related to previous claims of north–south asymmetry or localized abnormalities detected through wavelet techniques.

Key words: cosmic microwave background cosmology: theory methods: statistical

1 INTRODUCTION

Our picture of the Universe has evolved remarkably over the past century; from a view limited to our Galaxy to a cosmos with billions of similar structures. Today’s era of “precision cosmology”, cosmology appears to be concerned with improving estimates of parameters that describe the standard cosmological model rather than testing for possible alternatives. Recent observations of the large scale structure (eg. 2dFGRS; Percival et al. 2001) and the Wilkinson Microwave Anisotropy Probe (WMAP; Bennett et al. 2003a) observations of the Cosmic Microwave Background (CMB) appear to confirm our key ideas on structure formation. However, there is the suggestion that our confidence may be misplaced. The WMAP observations, for example, have thrown up a number of unusual features (Chiang et al. 2003; Efstathiou 2003; Naselsky, Doroshkevich & Verkhodanov 2003; Chiang & Naselsky 2004; Coles et al. 2004; Dineen & Coles 2004; Eriksen et al. 2004; Larson & Wandelt 2004; Park 2004; Land & Magueijo 2005a; Medeiros & Contaldi 2005).

In particular, it has been noted that the lowest spherical harmonics behave in a peculiar way, with an anomalously low quadrupole (see Efstathiou 2003, 2004) and confusion over the planar nature and alignment of the quadrupole and octopole (Tegmark, de Oliveira-Costa & Hamilton 2003; de Oliveira-Costa et al. 2004). Multipole vectors have also been used to show that there is preferred direction in the CMB sky (Copi, Huterer & Starkman 2004; Land & Magueijo 2005b). Wavelet techniques have demonstrated that particular regions in the sky display unusual characteristics (eg. Vielva et al. 2004; McEwen et al. 2005). Other statistical analyses give results that are compatible with Gaussianity (Colley & Gott 2003; Komatsu et al. 2003; Stannard & Coles 2005). There is some danger here of a “publication bias” in which only positive detections are reported so and it appears a good time to stand back from the established paradigm and systematically test the core assumptions intrinsic to our view of the universe.

Standard cosmological models assume the structures we see today grew from small initial perturbations through gravitational instability. The initial perturbations are thought to be seeded during a period of inflation (Guth 1981;

* E-mail: p.dineen@ic.ac.uk

Albrecht & Steinhardt 1982; Linde 1982). These primordial perturbations are the result of amplification of zero-point quantum fluctuations to classical scales during the inflationary period (Guth & Pi 1982; Hawking 1982; Starobinsky 1982). In most inflationary scenarios the resultant primordial density field is taken to be a statistically homogeneous and isotropic Gaussian random field (Adler 1981; Bardeen et al. 1986). Such a field has both physical and mathematical attractions. However, there are alternative possibilities that lead to a field with non-Gaussian statistics. Versions of inflation involving multiple scalar fields or those with non-vacuum initial states lead to a non-Gaussian spectrum. Other potential candidates for seeding the primordial field also lead to non-Gaussian possibilities. Topological defects arise from symmetries being broken as the early Universe cools. The topological defect scenario includes models based on cosmic strings, textures and monopoles (Kibble 1976; Vilenkin & Shellard 1994). The development of the defects involves nonlinear physics which leads to a non-Gaussian pattern of fluctuations.

The question of non-Gaussianity in the CMB is intertwined with the same question concerning the initial density perturbations. The inhomogeneity in the matter distribution is translated to the background radiation photons through Thomson scattering. After last scattering the majority of these photons arrive at our observatories unperturbed. If the primordial matter distribution is Gaussian then so too is the primary temperature pattern. Thus, the CMB anisotropies provides us with a clean tool to discriminate between initial field models described in the previous section. However, before we can test this assumption we need to ensure we are looking at the last-scattering surface. Most secondary anisotropies are nonlinear in nature and hence lead to non-Gaussian signals. Lensing and the Sunyaev-Zel'dovich effect should both be able to be isolated through their non-Gaussian effects. Moreover, both Galactic foregrounds and experimental systematic errors will leave non-Gaussian imprints in the CMB measurements. Thus, the development of non-Gaussian statistics that can isolate these effects is imperative. The demand for such tracers will only intensify: increased sensitivity and polarization measurements will require better control of secondary effects and foregrounds.

One of the primary goals of the WMAP mission is to make precise estimates of the cosmological parameters. These parameters are extracted by comparing the measured angular power spectrum to cosmological model predictions. The statistical information of the (processed) temperature field is assumed to be entirely encoded in the power spectrum, which is true if the field is a multivariate Gaussian. It is the aim of this paper to investigate this assumption: if it does not hold we may have to question the inferences obtained from the spectrum and address the causes of this non-normality whether cosmological, Galactic or systematic.

In this paper we approach this issue from a general statistical standpoint. Rather than looking for specific non-Gaussian alternatives we simply explore the extent to which the assumption of multivariate Gaussianity is supported by the data using the most general approaches available. The layout of the paper is as follows. In the next section we clarify the definition of a multivariate Gaussian random field. In Section 3, we outline techniques we shall use to probe the normality of current CMB data sets from WMAP. In Sec-

tion 4, we discuss the nature of the CMB data sets that the techniques are applied to. The details of the implementation of the method are drawn in 5. In Section 6, we present the results of our analysis. The conclusions are discussed in Section 7.

2 GAUSSIAN RANDOM FIELDS

Gaussian random fields arise in many situations that require the modelling of stochastic spatial fluctuations. There are two reasons for their widespread use. One is that the Central Limit Theorem requires that, under very weak assumptions, that linear additive processes tend to possess Gaussian statistics. To put this another way, the normal distribution is the least “special” way of modelling statistical fluctuations. The other reason is that Gaussian processes are fully specified in a mathematical sense. Very few non-Gaussian processes are as tractable analytically. The assumption of multivariate Gaussianity is consequently the simplest starting point for most statistical analyses.

If we signify the fluctuations in a Gaussian random field by $\delta(\mathbf{r}) = \delta$, then the probability distribution function of δ at individual spatial positions is given by

$$\mathcal{P}(\delta) = \frac{1}{(2\pi\sigma^2)^{1/2}} \exp\left(-\frac{\delta^2}{2\sigma^2}\right) \quad (1)$$

where σ^2 is the variance and δ is assumed to have a mean of zero. In fact, the formal definition of a Gaussian random field requires all the finite-dimensional p -variate joint distribution of a set of $\delta(\mathbf{r}_i) = \delta_i$ to have the form of a multivariate Gaussian distribution:

$$\mathcal{P}(\mathbf{\Delta}) = \frac{|\Sigma^{-1}|^{1/2}}{(2\pi)^{p/2}} \exp\left(-\frac{1}{2}\mathbf{\Delta}' \cdot \Sigma^{-1} \cdot \mathbf{\Delta}\right), \quad (2)$$

where $\mathbf{\Delta} = (\delta_1, \delta_2, \dots, \delta_p)'$ and Σ is the covariance matrix (Krzanowski 2000). Therefore, knowledge of the mean and variance of each variate, and all covariances between pairs of variates, fully specifies the field.

So how does this formalism manifest itself when we are dealing with the CMB? The temperature fluctuations $\Delta T(\theta, \phi)$ in the CMB at any point in the celestial sphere should be drawn from a multivariate Gaussian. That is to say, $\mathcal{P}(\Delta T_1, \Delta T_2, \dots, \Delta T_p)$ should have the same form of Equation 2. The CMB fluctuations can also be expressed in spherical harmonics as

$$\Delta T(\theta, \phi) = \sum_{\ell=1}^{\infty} \sum_{m=-\ell}^{m=+\ell} a_{\ell m} Y_{\ell m}(\theta, \phi), \quad (3)$$

where the $a_{\ell m}$ are complex and can be written

$$a_{\ell m} = |a_{\ell m}| \exp[i\varphi_{\ell m}]. \quad (4)$$

If the temperature field is a multivariate Gaussian then the real and imaginary parts of the $a_{\ell m}$ should be mutually independent and Gaussian distributed (Bardeen et al. 1986). Furthermore, the phases $\varphi_{\ell m}$ should be random. In our analyses we look for non-Gaussianity in the WMAP data in both real and harmonic spaces. Both spaces allows us to probe a range of length scales. Harmonic space has the advantage of being more condensed. Whereas, the advantage of studying

in real space is that we can easily navigate contaminated regions or focus on a specific area in the CMB sky. The exact nature of the data used is fully described in Section 4.

3 MULTIVARIATE ANALYSIS

In this Section, we outline the procedures used later to examine whether the WMAP data is strictly multivariate Gaussian. Generally, when looking for signs of non-normality, it helps to have an idea of the form it should take. The wide variety of possible sources of non-Gaussianity means that there is no unique form of alternative distribution to seek. Fortunately, this is quite a common problem in multivariate analyses, where real data does not adhere to any specific alternative model. This is unsurprising as there are very alternative models for which the entire hierarchy of multivariate distributions is fully specified. For this reason statisticians tend to apply not just one test statistic to the data, but a battery of complementary procedures. The assorted procedures will have differing sensitivities to the shape of the distribution. There is also a need to augment these tests with analyses of subsets of the data. Testing the form Equation 2 in all its generality is clearly impossible as it requires an infinite number of tests. In practice, various simplified approaches tend to be implemented: in particular, the one-point marginal distributions of the variates are often studied. Marginal normality does not imply joint normality, although the lack of multivariate normality is often reflected in the marginal distributions. A further advantage of examining the marginal distributions is that they are computationally less intense and more intuitive (i.e. easier to interpret) and thus more instructive.

The procedures we apply to the data are described in three subsections. In subsection 3.1, we outline univariate techniques for assessing marginal normality. In subsection 3.2, multivariate techniques for evaluating joint normality are sketched out. Lastly, we illustrate a procedure that evaluates the degree to which the regression of each variate on all others is linear in subsection 3.3. Throughout these subsections, we shall denote the members of the i th variate, \mathbf{x}_i , by x_{ij} where $j = 1, \dots, n$. In subsection 3.2, we shall use the notation $\mathbf{x}_j = (x_{1j}, x_{2j}, \dots, x_{pj})'$ and similarly $\mathbf{x}_k = (x_{1k}, x_{2k}, \dots, x_{pk})'$. We wish to emphasize the distinction between \mathbf{x}_j and $\mathbf{x}_i = (x_{i1}, x_{i2}, \dots, x_{in})'$.

3.1 Evaluating marginal normality

The evaluation of marginal normality of the data is based on well-known tests of univariate normality. The marginal distributions we study correspond to the distribution for each individual variate. This is simply the distribution of members of the specified variate, ignoring all other members from the data-set. For example, in the bivariate case, the marginal probability distribution of the variate \mathbf{x}_1 is given by

$$\mathcal{P}(\mathbf{x}_1) = \int_{-\infty}^{\infty} \mathcal{P}(\mathbf{x}_1, \mathbf{x}_2) d\mathbf{x}_2. \quad (5)$$

The parallel expression for the marginal distributions corresponding to larger values of the dimensionality p can easily

be developed. We outline four techniques that probe univariate normality of $\mathcal{P}(\mathbf{x}_i)$: the skewness and kurtosis coefficients; D'Agostino's omnibus test; and a shifted-power transformation test. In this subsection, we shall suppress the i indices when referring to the data-members such that x_j will refer to the individual members of \mathbf{x}_i .

The classic tests of normality is by means of evaluating the sample skewness $\sqrt{b_1}$ and kurtosis b_2 coefficients. If we let the sample mean and the sample variance be \bar{x} and S^2 respectively, and define

$$m_r = \frac{1}{n} \sum_{j=1}^n (x_j - \bar{x})^r, \quad (6)$$

to be the r^{th} moment about the mean. Then the skewness is given by

$$\sqrt{b_1} = \frac{m_3}{S^3}, \quad (7)$$

and the kurtosis by

$$b_2 = \frac{m_4}{S^4}. \quad (8)$$

The expected value of the skewness (Mardia 1980) is

$$E(\sqrt{b_1}) = 0, \quad (9)$$

and the square root of the variance of this quantity is

$$\sigma(\sqrt{b_1}) = \sqrt{\frac{6}{n}} \cdot \left(1 - \frac{3}{n} + \frac{6}{n^2} - \frac{15}{n^3} + \dots\right). \quad (10)$$

Here, and throughout the rest of the paper, we use the notation $E(Q)$ for the expected value of the statistic Q and $\sigma(Q)$ to signify the square root of the variance about this value. These values assume Q is applied to a Gaussian data-set. The same quantities for the kurtosis (Mardia 1980) are

$$E(b_2) = \frac{3(n-1)}{n+1}, \quad (11)$$

and

$$\sigma(b_2) = \sqrt{\frac{24}{n}} \cdot \left(1 - \frac{15}{2n} + \frac{271}{8n^2} - \frac{2319}{16n^3} + \dots\right). \quad (12)$$

So we have the expected value and variance of the kurtosis and skewness. But how useful are these quantities? Are we justified in using Gaussian statistics to measure non-normality? As the value of n increases the distribution of $E(\sqrt{b_1})$ soon reverts to a normal distribution. However, the distribution of $E(b_2)$ is very skewed for $n=100$ and is hardly normal for $n=1000$ (Mardia 1980). Clearly large values of n are required to be confident of the any analysis using the kurtosis. This last point is addressed further in Section 4 when our sample sizes are discussed.

There are a number of general tests that can be used to monitor the shape of the distribution of a variate. Some of these try to combine the skewness and kurtosis coefficients into an omnibus test. Other statistics aim to probe different features of the shape of the parent distribution. Using these statistics tend to be problematic as they usually require tabulated coefficients that are cumbersome and not available for large n . For this reason D'Agostino (1971) developed an omnibus test of normality for large sample sizes based on order statistics. The test statistic is defined as

$$D = \frac{1}{n^2 S} \sum_{j=1}^n \left(j - \frac{1}{2}(n+1) \right) x_{(j)}, \quad (13)$$

where $x_{(1)}, x_{(2)}, \dots, x_{(n)}$ are the n order statistics of the sample such that $x_{(1)} \leq x_{(2)} \leq \dots \leq x_{(n)}$. The expectation is

$$E(D) \simeq \frac{1}{2\sqrt{\pi}}, \quad (14)$$

and the variance asymptotically is given by

$$\sigma(D) = \frac{0.02998598}{\sqrt{n}}. \quad (15)$$

So far, we have looked at descriptive measures of the normality of the marginal distribution. There are also tests based on transforming the data. Box & Cox (1964) proposed using a shifted-power transformation to assess normality

$$x_j \rightarrow x_j^{(\xi, \lambda)} = \begin{cases} ((x_j + \xi)^\lambda - 1) / \lambda & \lambda \neq 0, x_j > -\xi \\ \log(x_j + \xi) & \lambda = 0, x_j > -\xi \end{cases} \quad (16)$$

The transformation aims to improve the normality of the variate x ; λ can be estimated by maximum likelihood and the null hypothesis, $H_0: \lambda = 1$, tested by a likelihood ratio test. The shift parameter ξ is included in the transformation because it appears to respond to the heavy-tailedness of the data, whereas, λ appears sensitive to the skewness (Gnanadesikan 1997). Specifically, it can be shown that the log-likelihood function is given by

$$\mathcal{L}_{\max}(\xi, \lambda) = -\frac{n}{2} \ln \hat{\sigma}^2 + (\lambda - 1) \sum_{j=1}^n \ln(x_j + \xi) \quad (17)$$

where $\hat{\sigma}^2$ is the maximum likelihood estimate of the transformed distribution that is presumed to be normal such that

$$\hat{\sigma}^2 = \frac{1}{n} \sum_{j=1}^n \left(x_j^{(\xi, \lambda)} - \bar{x}_j^{(\xi, \lambda)} \right)^2 \quad (18)$$

where

$$\bar{x}_j^{(\xi, \lambda)} = \frac{1}{n} \sum_{j=1}^n x_j^{(\xi, \lambda)} \quad (19)$$

Equation 17 is maximised to obtain the maximum likelihood estimates $\hat{\xi}$ and $\hat{\lambda}$. Finally, a significance test can be constructed by comparing the value of $2(\mathcal{L}_{\max}(\hat{\xi}, \hat{\lambda}) - \mathcal{L}_{\max}(\hat{\xi}, 1))$ to a χ^2 distribution with one degree of freedom. Note that $\mathcal{L}_{\max}(\xi, 1)$ is independent of ξ so this is a free parameter in the test.

3.2 Evaluating joint normality

As we have already remarked, deviations from joint normality should be detectable through methods directed toward testing the marginal normality of each variate. However, there is a need to explicitly test the multivariate nature of the data. Therefore, we look at three techniques that fulfil this requirement. These techniques are multivariate generalizations of univariate tests outlined in Section 3.1.

The first two techniques to evaluate joint normality are multivariate measures of skewness and kurtosis. These methods were developed by Mardia (1970) and make use of Mahalanobis distance of \mathbf{x}_j and Mahalanobis angle between $\mathbf{x}_j - \bar{\mathbf{x}}$ and $\mathbf{x}_k - \bar{\mathbf{x}}$. The Mahalanobis distance is defined as

$$r_j^2 = (\mathbf{x}_j - \bar{\mathbf{x}})' \mathbf{S}^{-1} (\mathbf{x}_j - \bar{\mathbf{x}}), \quad (20)$$

where \mathbf{S} is the sample covariance matrix. It is often used to assess the similarity of two or more data sets. The Mahalanobis angle is given by

$$r_{jk} = (\mathbf{x}_j - \bar{\mathbf{x}})' \mathbf{S}^{-1} (\mathbf{x}_k - \bar{\mathbf{x}}). \quad (21)$$

The multivariate skewness is related to the Mahalanobis angle and as such reflects the orientation of the data. It is defined as

$$b_{1p} = \frac{1}{n^2} \sum_{j=1}^n \sum_{k=1}^n r_{jk}^3, \quad (22)$$

where $nb_{1p}/6$ is asymptotically distributed as a χ^2 with $p(p+1)(p+2)/6$ degrees of freedom. In the bivariate case, this is a χ^2_4 distribution. The multivariate kurtosis is defined as the mean of the square of the Mahalanobis distance

$$b_{2p} = \frac{1}{n} \sum_{j=1}^n r_j^4. \quad (23)$$

It is expected to be normally distributed with mean $p(p+2)$ and variance $8p(p+2)/n$. Therefore, we have $E(b_{22}) = 8$ and $\sigma(b_{22}) = \sqrt{64/n}$.

Our last multivariate technique is an extension of the transformation test. We simply look at just the power transformation of each variable separately ignoring the shift parameter ξ . That is to say

$$\mathbf{x}_i \rightarrow \mathbf{x}_i^{(\lambda)} = \begin{cases} (x_{ij}^{\lambda_i} - 1) / \lambda_i & \lambda_i \neq 0 \\ \log(x_{ij}) & \lambda_i = 0 \end{cases} \quad (24)$$

The maximised log-likelihood function is given by

$$\mathcal{L}_{\max}(\lambda) = -\frac{n}{2} \ln |\hat{\Sigma}| + \sum_{i=1}^p \left[(\lambda_i - 1) \sum_{j=1}^n \ln x_{ij} \right], \quad (25)$$

where $\hat{\Sigma}$ is maximum likelihood estimate of the covariance matrix of the transformed data (Gnanadesikan 1997). $\hat{\Sigma}$ is computed in analogous fashion to $\hat{\sigma}^2$ in Equation 17. The transformation with $\lambda = (\lambda_1, \dots, \lambda_p)' = \mathbf{1}$ is the only transformation consistent with normality. Therefore, as with the univariate case, we can compare the value of $2(\mathcal{L}_{\max}(\hat{\lambda}) - \mathcal{L}_{\max}(\mathbf{1}))$ to a χ^2_p distribution.

3.3 Evaluating linearity

There is a further aspect of multivariate normality that we can examine in our data set: all variates, if not independent of each other, should be linearly related. Here we are not specifically testing the normality of the variates, as it is easy to imagine variates that are extremely non-normal yet linearly related (eg. two identical sawtooth distributions). Importantly though, any non-linearity does inform us about the usefulness of the covariance matrix. Whereas, marginal non-normality may allow you to still extract useful information from the covariance matrix. Non-linearity results in the more serious consequence of the covariance matrix being a poor indicator, even qualitatively, of the association of variates (Cox & Small 1978). Our prime motivation for assessing the multivariate Gaussianity of the WMAP data is due to statistical nature of the data underpinning the extraction of cosmological parameters. It is therefore essential

that the covariance matrix fully specifies all the information from the data set. Clearly, testing linearity is not only complementary to the previous tests we have outlined, but also can be thought of as a vital step in assessing the Gaussianity of CMB data.

Investigating the linearity of regression of variates as a means of scrutinizing multivariate normality was first proposed by Cox & Small (1978). We shall outline a related method for obtaining and evaluating regression coefficients described in Montgomery (1997). To begin with, let us look at the general concepts behind multiple linear regression. If we have n measurements of two variables y and z , then, the two variables are related linearly when the following model fully describes their relationship

$$y_j = A_0 + A_1 z_j + \epsilon_j, \quad (26)$$

where ϵ_j is the error term in the model and (as usual) the subscript j runs from 1 to n . The parameters A_α are referred to as regression coefficients. We can consider building other terms into our model

$$y_j = A_0 + A_1 z_{j1} + A_2 z_{j2} + \dots + A_q z_{jq} + \epsilon_j, \quad (27)$$

where $z_{j\alpha}$ can be z_j^2 , $z_j y_j$, $z_j^{1/3}$ and so on. Linearity dictates that the regression coefficients A_α should be zero for all non-linear terms. So how do we estimate A_α ? A typical technique is to minimize the error term ϵ_j . If we rewrite Equation (27) in matrix notation, we have

$$\mathbf{y} = \mathbf{Z}\mathbf{A} + \boldsymbol{\epsilon} \quad (28)$$

where $\mathbf{A} = (A_0, \dots, A_q)'$ and \mathbf{Z} is a $n \times (q+1)$ matrix with the first column comprised of ones and the subsequent columns corresponding to k regressor variables in the model. The error term can be minimized using the method of least-squares. The least-squares function is given by

$$L = \sum_{j=1}^n \epsilon_j^2 = \boldsymbol{\epsilon}'\boldsymbol{\epsilon} = (\mathbf{y} - \mathbf{Z}\mathbf{A})'(\mathbf{y} - \mathbf{Z}\mathbf{A}). \quad (29)$$

Differentiating Equation 29 with respect to \mathbf{A} and equating this to zero, minimizes this function and leads us to

$$\hat{\mathbf{A}} = (\mathbf{Z}'\mathbf{Z})^{-1} \mathbf{Z}'\mathbf{y}, \quad (30)$$

which is our best estimate of \mathbf{A} .

Once we have obtained a set of regression coefficients, we wish to test the significance of each coefficient. If the variables are linearly related then the coefficients for the additional coefficients to our model should be zero. Given an individual coefficient A_α , we therefore want to check the hypothesis $H_0: A_\alpha = 0$ against $H_1: A_\alpha \neq 0$. If H_0 is not rejected for one of the additional coefficients, then the term needs to be added to model the behaviour of the variables. Montgomery (1997) outlines a statistic t_0 that can be used to test this hypothesis. The error in our estimate of $\hat{\mathbf{A}}$ is given by

$$\hat{\sigma}^2 = \frac{1}{n-q} \cdot (\mathbf{y}'\mathbf{y} - \hat{\mathbf{A}}'\mathbf{Z}'\mathbf{y}). \quad (31)$$

The test statistic for H_0 is

$$t_0 = \frac{\hat{A}_\alpha}{\sqrt{\hat{\sigma}^2 C_{\alpha\alpha}}} \quad (32)$$

where $C_{\alpha\alpha}$ is the diagonal element of $(\mathbf{Z}'\mathbf{Z})^{-1}$ corresponding

to A_α . The statistic t_0 should match a t -distribution with $(n - q - 1)$ degrees of freedom.

4 DATA

The WMAP instrument comprises 10 differencing assemblies (consisting of two radiometers each) measuring over 5 frequencies ($\sim 23, 33, 41, 61$ and 94 GHz). The two lowest frequency bands (K and Ka) are primarily Galactic foreground monitors, while the highest three (Q , V and W) are primarily cosmological bands (Hinshaw et al. 2003).

In our study, we look at a total of 15 maps constructed from the WMAP data. All the maps were obtained from the NASA's LAMBDA[†] data archive. The maps are in HEALPix[‡] format with a resolution parameter of $N_{\text{side}}=512$. The data consists of: 5 frequency maps; 8 'foreground-cleaned' assembly maps; and 2 CMB-only maps. We shall refer to these sets of maps as sets (a), (b) and (c), respectively. Set (a) is composed of five maps corresponding to each frequency bandpasses observed by WMAP. For each pixel in these maps, noise weighting is used to compute the average temperature from the individual differencing assembly map values. Set (b) consists of 'foreground-cleaned' sky maps corresponding to each individual differencing assembly. The assemblies are labelled $Q1$, $Q2$, $V1$, $V2$, $W1$, $W2$, $W3$ and $W4$, where the letter corresponds to the frequency band. These maps were used in the calculation of the angular power spectrum by the WMAP team (Hinshaw et al. 2003). The Galactic foreground signal was removed using a 3-band, 5-parameter template fitting method described in Bennett et al (2003b). Set (c) corresponds to two CMB-only maps constructed by the WMAP team (Bennett et al. 2003b) and Tegmark, de Oliveira-Costa & Hamilton (2003) (see papers for details). We shall refer to these two maps as the ILC and TOH maps, respectively. Both maps were assembled in a manner that minimises foreground contamination and detector noise, leaving a pure CMB signal. The ultimate goal of these two maps is to build an accurate image of the last-scattering-surface that captures the detailed morphology.

For CMB analyses, it is necessary to mask out regions of strong foreground emission. Bennett et al. 2003b provide masks for excluding regions where the contamination level is large. The masks are based on the K -band measurements, where contamination is most severe. The severity of the mask is a compromise between eliminating foregrounds and maximising sky area in analyses. In our analysis, we concentrate our statistics on maps with the kp2 mask applied. This results in 15.0% of pixels being cut. When set (b) is combined with the kp2 mask, we replicate the data used in the calculation of the angular power spectrum. The Galactic sky cut is unnecessary when looking at set (c) as the whole sky should be uncontaminated, however, we still apply the cut for consistency and simplicity. We also occasionally refer to results with the application of the kp0 mask which excludes 23.0% of the sky.

[†] <http://lambda.gsfc.nasa.gov>

[‡] <http://healpix.jpl.nasa.gov>

5 IMPLEMENTATION

In order to keep our study as focussed as possible, our initial multivariate test is bivariate: simply involves looking at pairs of variates extracted from the maps. This allows us to use the same methods on both real and harmonic space quantities as we shall explain later in this section. The study of bivariate has the additional benefit of reducing the computational requirements. However, we should emphasise that all the methods outlined in Section 3 are applicable to larger values of p . For a pair of variates $(\mathbf{x}_1, \mathbf{x}_2)$, we assess the normality of the bivariate probability distribution $\mathcal{P}(\mathbf{x}_1, \mathbf{x}_2)$. The probability distribution should have the form outlined in Equation 2. In real space, we look at temperature pairs $(\Delta T_1, \Delta T_2)$. This allows us to assess the 2-point correlation function if we extract pixel pairs across a range of scales. We randomly select 1 million temperature pairs from a given map. As there are roughly 3 million pixels, it means that there are $\sim 10^{13}$ combinations of pairs. We found that a million pairs were sufficient to replicate the overall distribution. We then calculate the angular separation of each pair. The pairs are then grouped into 100 bins according to their separation such that the bin sizes are roughly equal. Thus, we are left with 100 bins with $n \sim 10,000$. In harmonic space, we study the distribution of the real \Re and imaginary \Im parts of the spherical harmonic coefficients. This idea could be extended to different mode functions. Spherical harmonic modes are independent for a Gaussian random field defined on a sphere. The effect of a cut or other mask is to correlate these models, but only through the introduction of a linear covariance. This means that this method could be used to study any combination of modes even on a cut sky.

One of the other advantages of looking in harmonic space is that it is trivial to probe differing scale lengths. We simply study the distribution of (\Re, \Im) for a given value of ℓ . Consequently, we have bins with $n = \ell$. We probe scales up to and including $\ell = 600$, however, due to the small value of n at low ℓ we ignore the results for $\ell < 100$. However, the effect of using masks on sets (a) and (b) means that the harmonic coefficients cannot easily be calculated. Thus, we only study harmonic space for set (c) where the whole-sky can be appropriately studied.

We now outline how the various statistics were computed for bivariate data. The skewness, kurtosis and D'Agostino's statistics, applied to the marginal distributions, are trivial to calculate. As we have already mentioned, there is an issue with distribution of the expected kurtosis $E(b_2)$ being non-Gaussian for small n . This is not an issue in real space where n is very large, but, it is worth bearing in mind in harmonic space. We could address this issue by modelling the distribution of $E(b_2)$ using Monte Carlo simulations. However, as this is only an issue for a small part of our analysis and require significantly more computation we chose not to adopt this method. The univariate shifted-power transformation method is more challenging to implement. The method requires a careful choice of minimiser/maximiser. The majority of minimizers call for the derivative of the function being minimized. The derivative of Equation (17) is computationally taxing. Therefore, we choose to use a 'simplex downhill' minimizer (Press et al. 1992) that requires only the actual function. The simplex minimizer is applicable to multidimensional functions which

fulfils our need for minimizing a 2-dimensional function. Most minimizers do not find the global minimum, instead they get 'trapped' in local minima. We allow for this by testing our code with various initial starting points along the function and varying the step size. Nevertheless, there is still the possibility that we may fail to find the true minimum, especially if the shape of the function is complex. Indeed, evidence is found that we fail to obtain the global minimum in some of our results (see later). However, we are not unduly worried by this since a local minimum will result in smaller value of $2(\mathcal{L}_{\max}(\hat{\xi}, \hat{\lambda}) - \mathcal{L}_{\max}(\hat{\xi}, 1))$ than that calculated from the true minimum. Thus, we will fail to detect non-normality rather than falsely claim non-normality.

The bivariate skewness and kurtosis are simple to calculate. However, the bivariate power transformation method has the same challenges as in the univariate case. Again, we are trying to minimize a 2-dimensional function and so we turn to the simplex minimizer. Obviously, by using this minimizer we inherit the same problems as for the univariate transformation.

Finally, we look at the linearity of the temperature pairs and (\Re, \Im) pair. We add separately three non-linear terms to our model of the data:

$$\begin{aligned} x_{2j} &= A_0 + A_1 x_{1j} + A_2 x_{1j}^2 \\ x_{2j} &= A_0 + A_1 x_{1j} + A_2 x_{1j}^3 \\ x_{2j} &= A_0 + A_1 x_{1j} + A_2 / x_{1j} \end{aligned} \quad (33)$$

where, as before, x_{ij} are elements from the variate \mathbf{x}_i . Our task is now simply to assess the significance of the coefficient A_2 for the three non-linear terms using Equation (32).

6 RESULTS

In this section, we present the results of our analysis on the WMAP-derived data. Throughout the section, the expectation value of a statistic $E(Q)$, if non-zero, is marked in the figures as a straight line. The dark grey areas in the plots represent the 95% confidence regions. For example, if the distribution of $E(Q)$ is (or approximates for large n) a normal distribution, then the dark grey region signifies $E(Q) \pm 1.95996\sigma$. The light grey region is the 99% confidence region. In section 6.1, we display and discuss the results of applying our statistics to temperature pairs from the assembly maps, the frequency maps, the CMB-only maps and a sample Gaussian Monte Carlo (MC) map. The latter map is used as a reference guide and to reassure us that the computation of a statistic is accurate. For each map, the statistics were applied to 100 binned distributions and therefore we expect one value (for each statistic) to be outside the 99% confidence region. In section 6.2, we discuss the same analysis on the spherical harmonic coefficients obtained from the CMB-only maps and the same sample Gaussian MC map. For each map, the statistics are applied to 501 distributions ($\ell = 100 - 600$) and as such we expect 5 points beyond the 99% confidence region.

6.1 Real Space

6.1.1 Marginal normality results

The results of the application of the univariate methods on the temperature pairs are displayed in Figures 1-8. We dis-

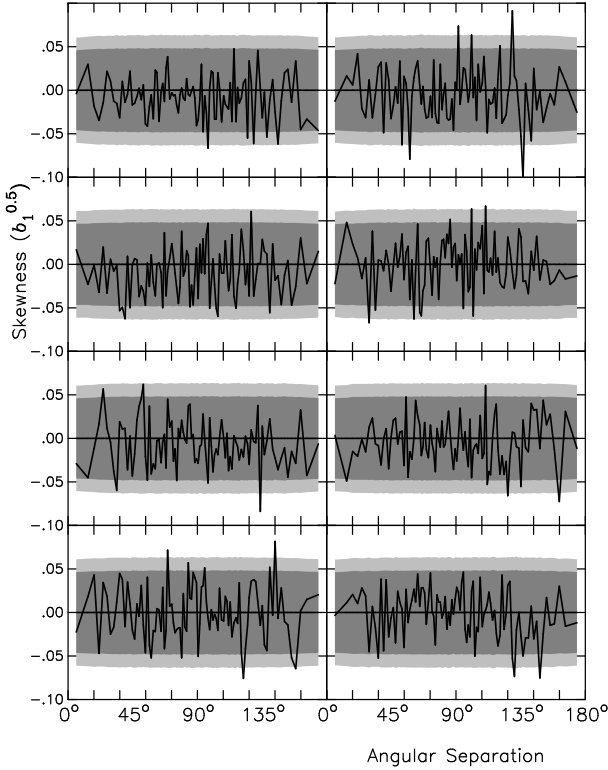


Figure 1. Skewness results from the foreground-cleaned assembly maps. (Top left) Q1 assembly map, (top right) Q2 assembly map, (2nd from top, left) V1 assembly map, (2nd from top, right) V2 assembly map, (3rd from top, left) W1 assembly map, (3rd from top, right) W2 assembly map, (bottom, left) W3 assembly map, and (bottom, right) W4 assembly map.

play the results for ΔT_1 to increase clarity, although unsurprisingly, the corresponding plots for ΔT_2 resemble those for ΔT_1 .

The skewness results are shown in Figures 1 and 2. The assembly data shows no signs of being skewed. However, the two non-cosmological frequencies (K and Ka) are very skewed. Clearly, the maps are heavily contaminated with Galactic foregrounds even outside the kp2 cut. Moreover, the construction of the kp2 mask means that the shape of the distribution of K has an artificial cut-off at high ΔT . The skewness coefficients appear uniform across all angular separations. Looking at the results from the cosmological frequencies, the Q band frequency appears slightly positively skewed but the two higher frequency display no sign of non-normality. Interestingly, when we look at the CMB-only maps, the TOH map appears negatively skewed- there are roughly 15 points outside the 99% confidence region. This is the opposite sign to the two non-cosmological bands which may suggest that the foreground-removal process has resulted in an over-subtraction. The ILC map also appears to be slightly negatively skewed.

The analyses of the kurtosis coefficient are shown in Figures 3 and 4. The kurtosis is higher than expected in all 8 assembly maps and across all angular separations. The kurtosis is even greater in the non-cosmological frequency maps suggesting that not all the foreground information has been removed from the assembly maps. The two CMB-only maps also hint at this but with less certainty. Both maps

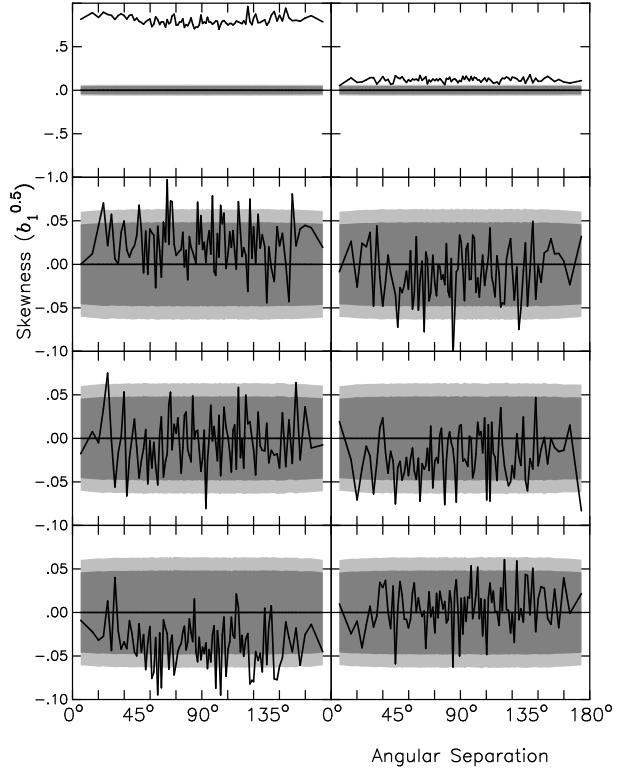


Figure 2. Skewness results from the 5 frequency maps, the 2 CMB-only maps and a Gaussian MC map. (Top left) K band map, (top right) Ka band map, (2nd from top, left) Q band (2nd from top, right) V band map, (3rd from top, left) W band map, (3rd from top, right) ILC CMB-only map, (bottom, left) TOH CMB-only map, and (bottom, right) a Gaussian MC map.

have a slightly higher than expected kurtosis especially when the two are compared to results from the Gaussian MC map. That is to say, their distributions are too peaked, and as with the skewness results suggests errors in foreground modelling.

D'Agostino's test statistic is shown in Figures 5 and 6. The statistic is an omnibus statistic so it should be unsurprising that it also pick up evidence of non-normality in all the WMAP-derived maps. Again, the results from the assembly maps have values mainly outside the 99% confidence region. This shift away from the expected value is even greater for the K and Ka bands. The three cosmological frequency maps produce results that appear non-normal but with much less significance than the Galactic bands. The two CMB-only maps also appear non-normal. At this point, we note that both the kurtosis and D'Agostino's statistic have a greater shift away from their expected values for the Galactic frequencies for the very large and very small angles. This feature is seen later on in the other statistics we employ.

The results of the shifted-power transformation of the data sets are shown in Figures 7 and 8. This part of our analysis was the most computationally challenging aspect, therefore, we are pleased to see that the result from the Gaussian MC map is as expected. Due to the challenge of this part of work we really look for severe departure from non-normality and keep our discussion brief. The assembly maps appear to have slightly more than expected points beyond the 99% confidence region. Moreover, the two non-cosmological frequency maps show clear signs of non-normality. The two

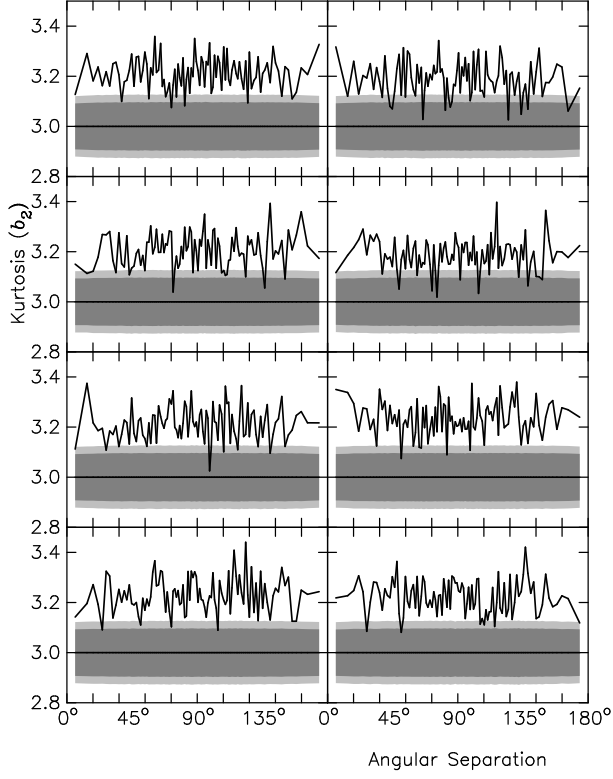


Figure 3. Kurtosis results from the foreground-cleaned assembly maps.

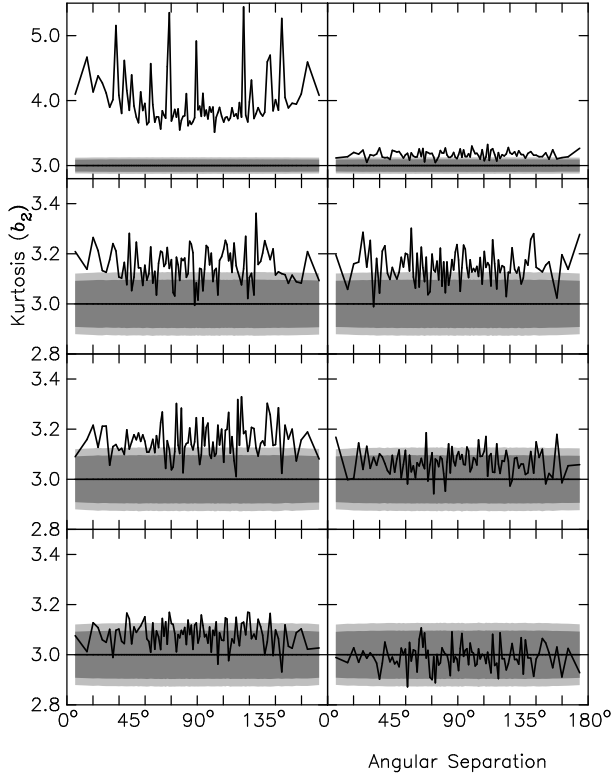


Figure 4. Kurtosis results from the 5 frequency maps, the 2 CMB-only maps and a Gaussian MC map.

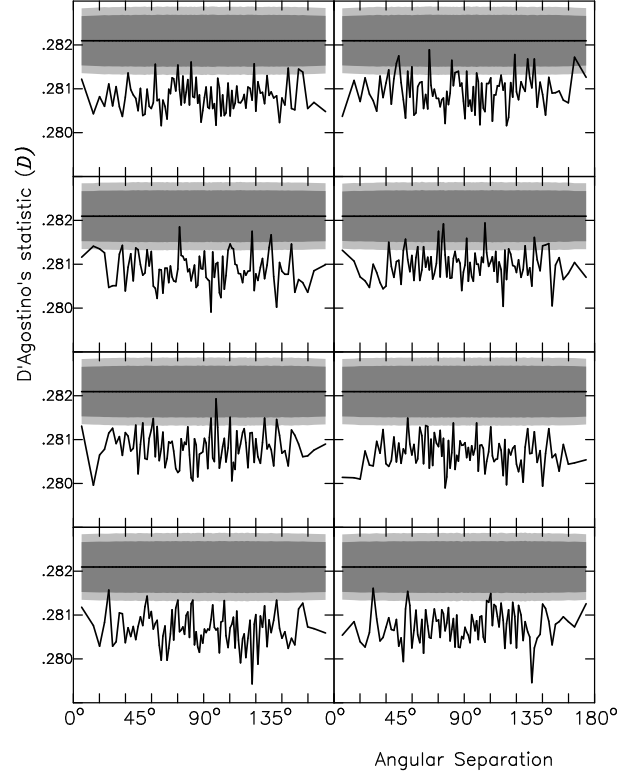


Figure 5. D'Agostino's statistic results from the foreground-cleaned assembly maps.

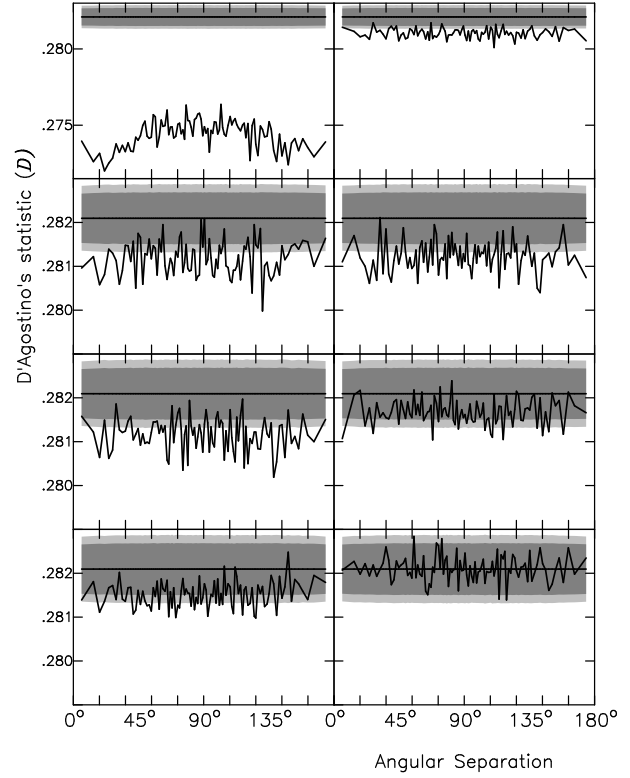


Figure 6. D'Agostino's statistic results from the 5 frequency maps, the 2 CMB-only maps and a Gaussian MC map.

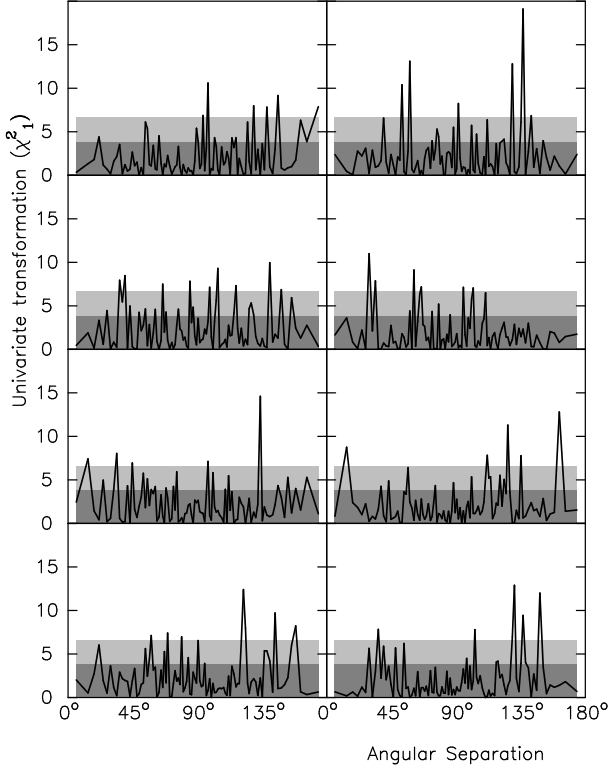


Figure 7. Univariate transformation results from the foreground-cleaned assembly maps.

CMB-only maps also show signs of non-normality- the TOH map result appearing to have departed furthest from normality.

6.1.2 Joint normality results

Our bivariate analysis results are shown in Figures 9-14. The bivariate skewness statistics ($nb_{12}/6$) calculated from the 16 maps are shown in Figures 9 and 10. The statistic appears to be abnormal for three of the assembly maps- *Q1*, *W2* and *W4*. Some of the other assembly maps have two or three points outside the 99% confidence region but visually the results do not look too unusual. Once again, the two non-cosmological frequencies have results that strongly indicate non-normality. This non-normality is still evident in the *Q* and *V* band. The two CMB maps also have a higher than expected number of points above the 99% confidence region. It would appear that the bivariate skewness results mimic their univariate counterparts.

The bivariate kurtosis results are displayed in Figures 11 and 12. As with the skewness results, bivariate kurtosis seem similar to their univariate equivalent. Nevertheless, in the case of the assembly maps, the shift away from the expected value is even greater than for the univariate results. As before, the Galactic frequency maps are clearly found to be non-normal. The higher value than expected value of the bivariate kurtosis persists in the foreground-cleaned CMB maps

The bivariate power transformation is shown in Figures 13 and 14. The assembly results do not look entirely consistent with being drawn from a χ^2_2 distribution. Five of the

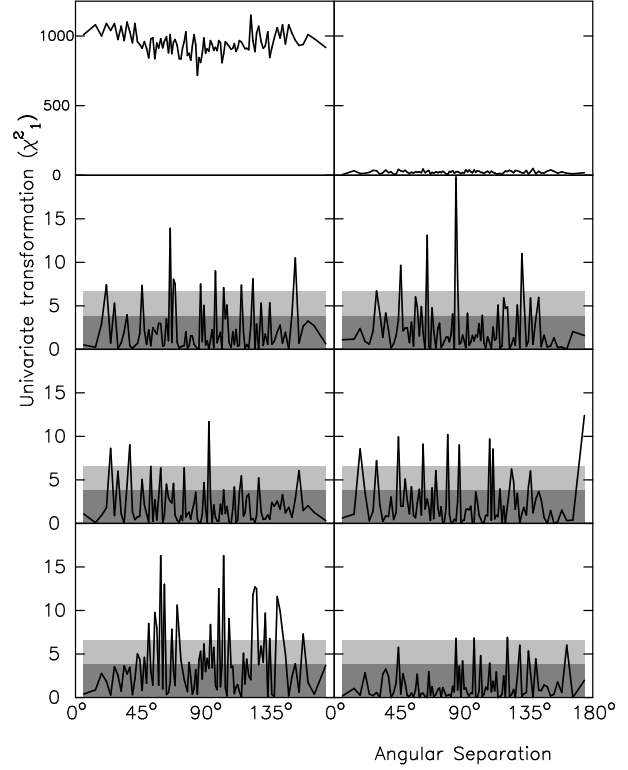


Figure 8. Univariate transformation results from the 5 frequency maps, the 2 CMB-only maps and a Gaussian MC map.

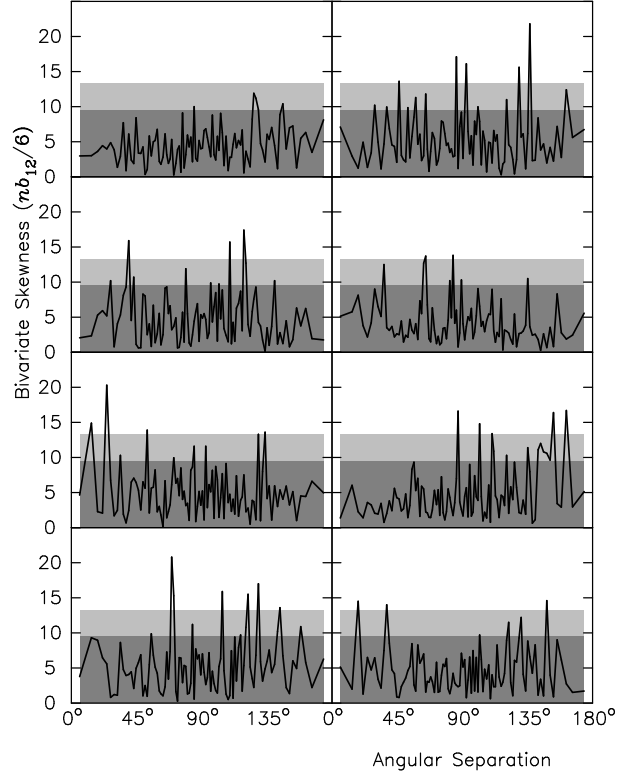


Figure 9. Bivariate skewness results from the foreground-cleaned assembly maps.

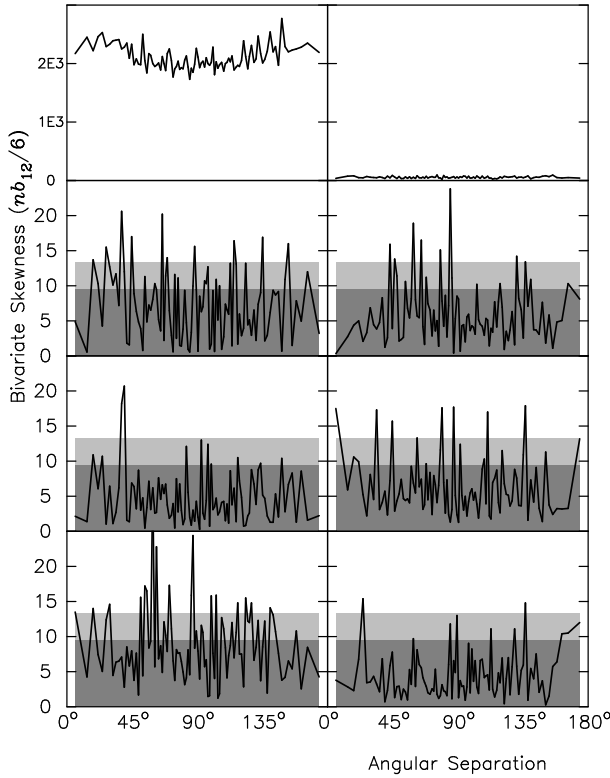


Figure 10. Bivariate skewness results from the 5 frequency maps, the 2 CMB-only maps and a Gaussian MC map.

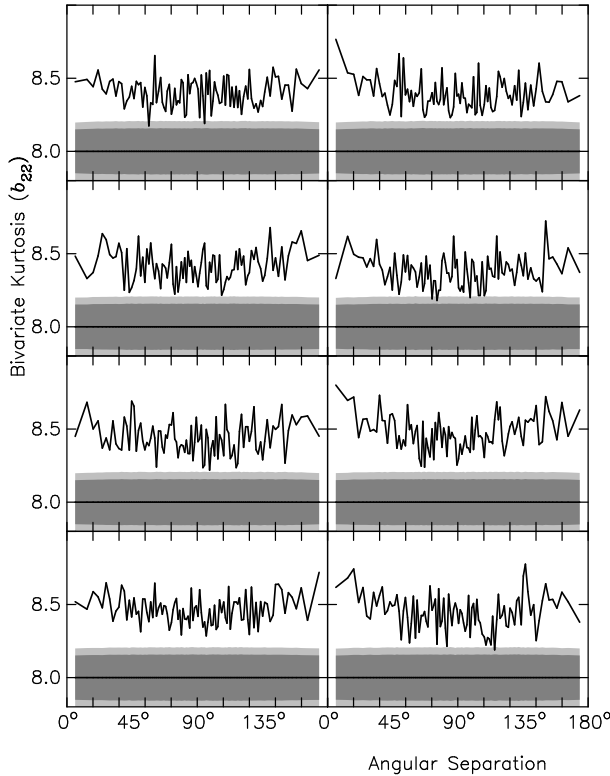


Figure 11. Bivariate kurtosis results from the foreground-cleaned assembly maps.

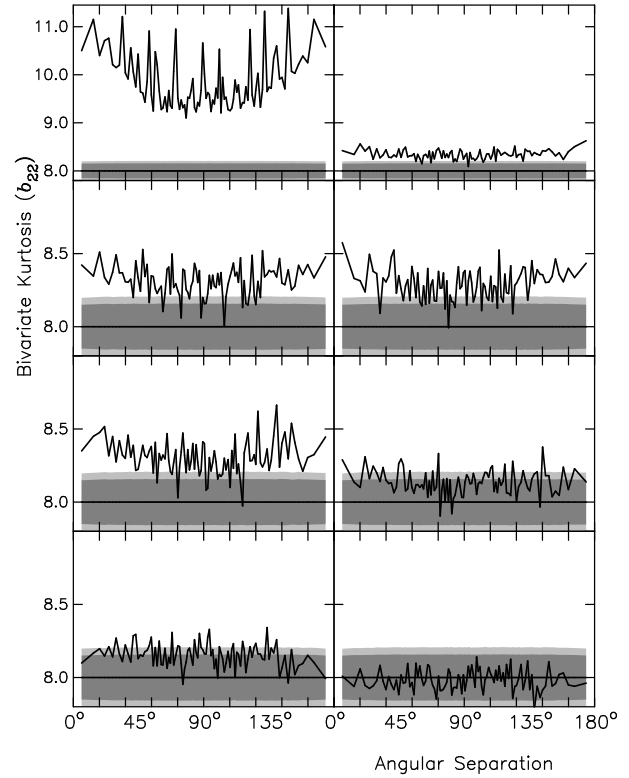


Figure 12. Bivariate kurtosis results from the 5 frequency maps, the 2 CMB-only maps and a Gaussian MC map.

assembly maps produce results with 5 or more points outside the 99% confidence region. Saying that, our Gaussian MC map has four points outside this region, which makes it hard to draw definite conclusions. This is certainly not true for the two Galactic frequency bands that are clearly inconsistent with normality. The two CMB-only maps also appear to have an extremely high number of points beyond the 99% confidence region.

6.1.3 Linearity results

Lastly, in this subsection, we assess the linearity of the data. We tried adding separately three non-linear terms to our linear model of the data (as described in 5). However, all three terms were found to be unnecessary descriptors for the data from all of the maps bar the heavily contaminated K band map. This is reassuring as it tells us that the angular power spectrum supplies reliable information about the data sets. We plot in Figures 15 and 16 the results for addition of the z_j^2 non-linear term. Curiously, the non-linearity seen in the K band map is seen at the largest and very smallest angular separations. As has already been noted, this trend is seen in other statistics that we employ.

6.2 Harmonic space

6.2.1 Marginal normality results

The results of applying the skewness, kurtosis and D'Agostino's statistics are shown in Figures 17, 18 and 19,

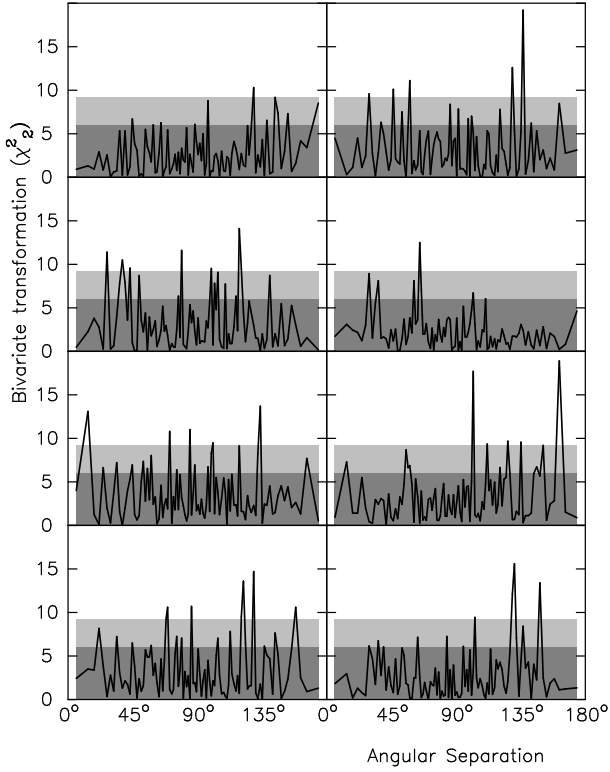


Figure 13. Bivariate transformation results from the foreground-cleaned assembly maps..

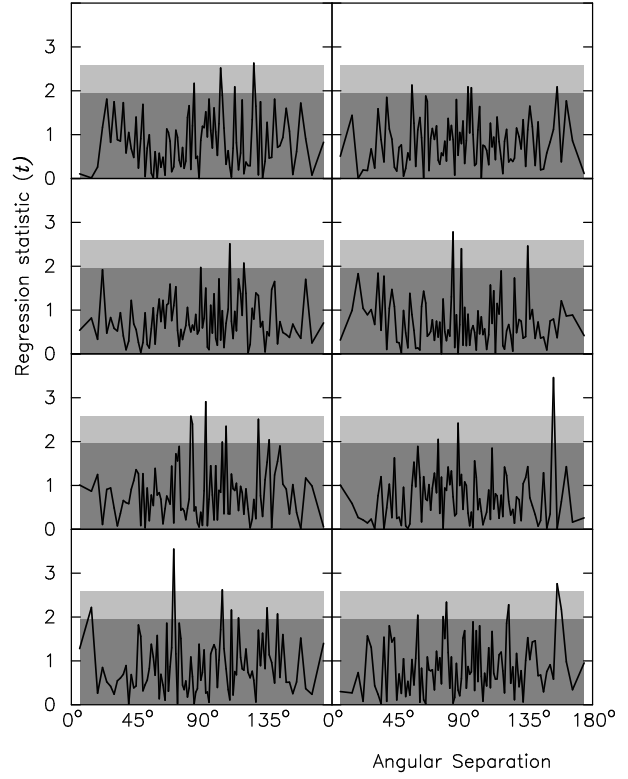


Figure 15. Linear regression results from the foreground-cleaned assembly maps.

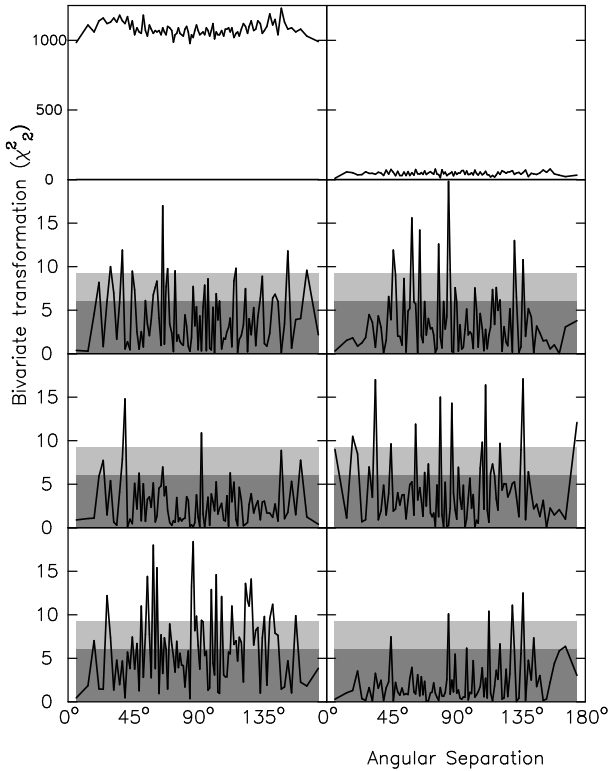


Figure 14. Bivariate transformation results from the 5 frequency maps, the 2 CMB-only maps and a Gaussian MC map.

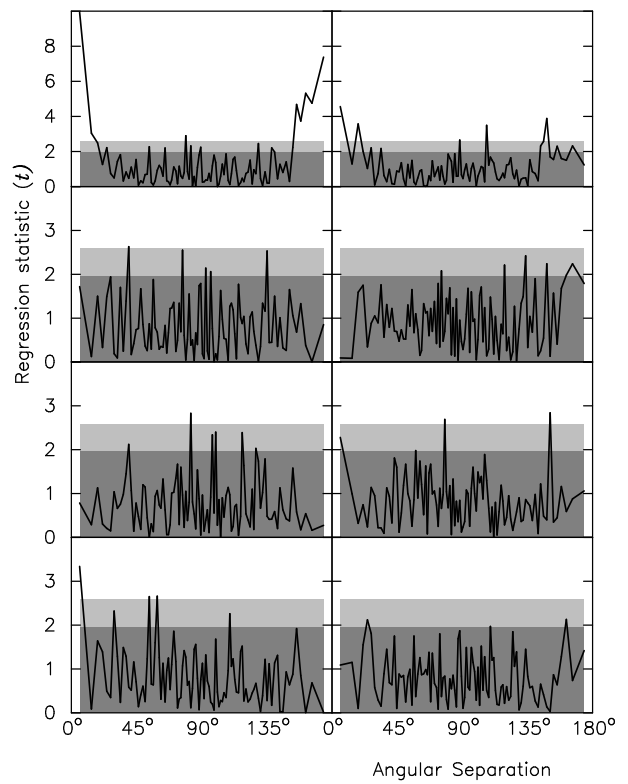


Figure 16. Linear regression results from the 5 frequency maps, the 2 CMB-only maps and a Gaussian MC map.

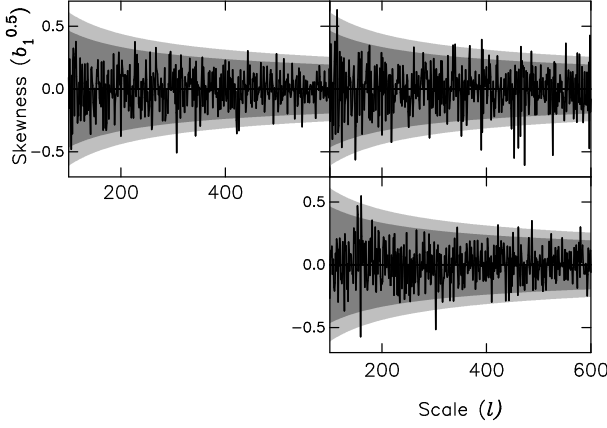


Figure 17. Skewness results from the $a_{\ell m}$ of the 2 CMB-only maps and a Gaussian MC map. (Top left) ILC CMB-only map, (top right) TOH CMB-only map and (bottom) a Gaussian MC map

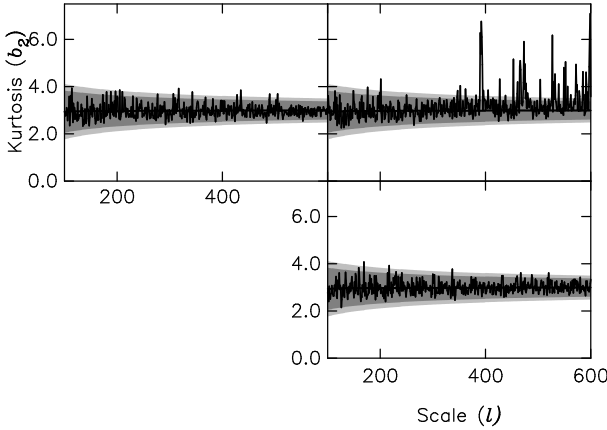


Figure 18. Kurtosis results from the $a_{\ell m}$ of the 2 CMB-only maps and a Gaussian MC map.

respectively. The results from the ILC map appear consistent with normality. However, all three statistics behave unusually for the TOH map on scales smaller than $\ell \sim 400$. This is particularly true of the kurtosis coefficient where the non-normality is most evident. It would be interesting to relate this non-normality to that already seen in real space. This could hopefully give us a better handle on the source of the non-Gaussianity (whether Galactic or cosmological). The univariate transformation results are shown for completeness in Figure 20. However, the method appears unreliable as the Gaussian MC map results are inconsistent with being drawn from a χ^2_1 distributions. We feel this unreliability is due to the small values of n that make the minimized function shape more complex.

6.2.2 Joint normality results

The application of our bivariate skewness and kurtosis statistics are shown in Figures 21 and 22. Once again, the ILC map behaviour corresponds to that of the Gaussian MC map. However, the TOH map shows clear signs of non-normality. The non-normality is displayed from larger scales

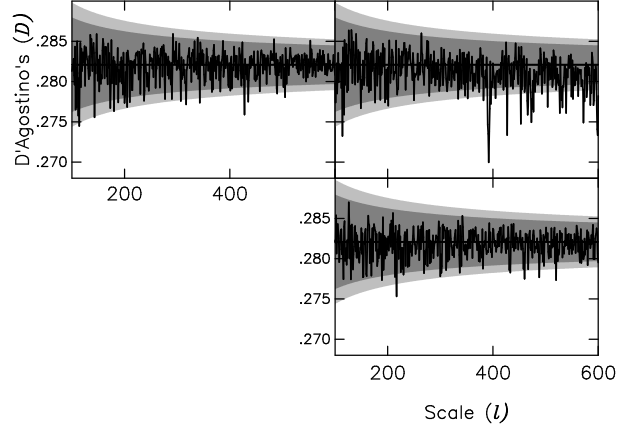


Figure 19. D'Agostino's statistic results from the $a_{\ell m}$ of the 2 CMB-only maps and a Gaussian MC map.

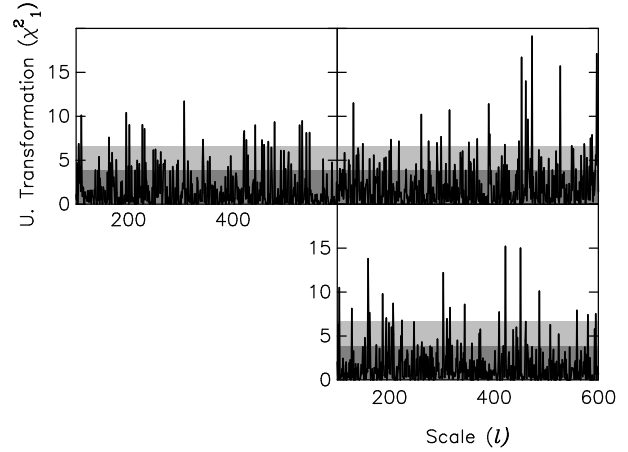


Figure 20. Univariate transformation results from the $a_{\ell m}$ of the 2 CMB-only maps and a Gaussian MC map.

than the univariate counterparts. That is to say, the distribution of the $a_{\ell m}$ s appears unusual at scales greater than $\ell = 300$. The results from the multivariate power transformations using harmonic space data are shown in Figure 23. Looking at the results from the ILC and Gaussian MC maps, it appears that we are failing to find the true global minimum. As discussed earlier, finding a local minimum will result in an underestimate of the value of χ^2_2 . Therefore, we are not too concerned about this as failure to find global minima since it failure does not result in false claims of non-Gaussianity. Intriguingly, the shape of the line for the TOH map does not match those of the other two maps. If we are failing to find the global minima then we would expect a larger number of points to be beyond the 99% confidence region if we corrected this failure. Equally, the result may reflect that the distributions extracted from the TOH maps make finding the global minimum easier because they are, to some extent, smoother.

6.2.3 Linearity results

In our analysis of the linearity of the harmonic space variates, we do not find any evidence of non-linearity. This was

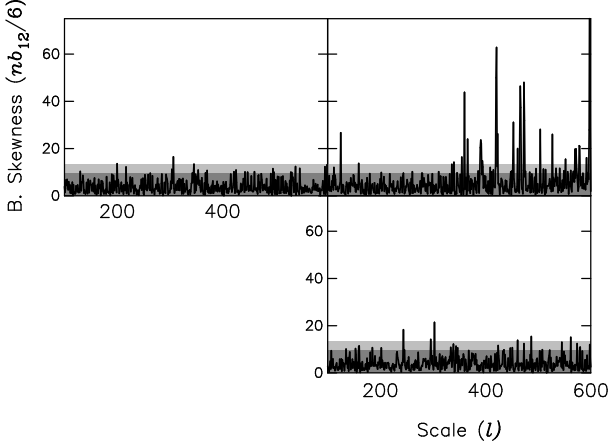


Figure 21. Bivariate skewness results from the $a_{\ell m}$ of the 2 CMB-only maps and a Gaussian MC map.

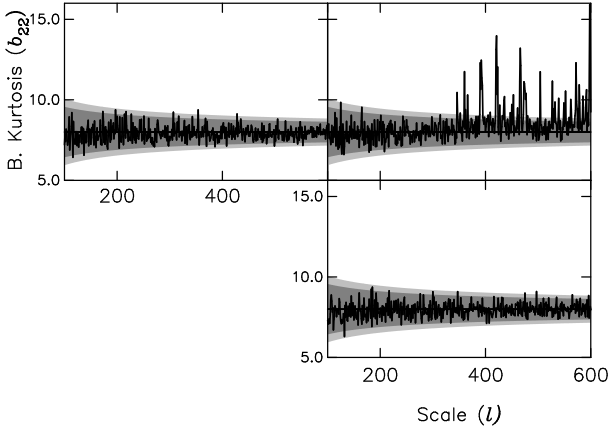


Figure 22. Bivariate kurtosis results from the $a_{\ell m}$ of the 2 CMB-only maps and a Gaussian MC map.

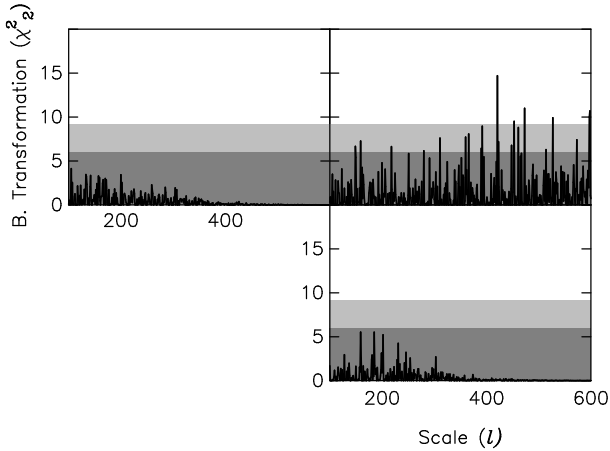


Figure 23. Bivariate transformation results from the $a_{\ell m}$ of the 2 CMB-only maps and a Gaussian MC map.

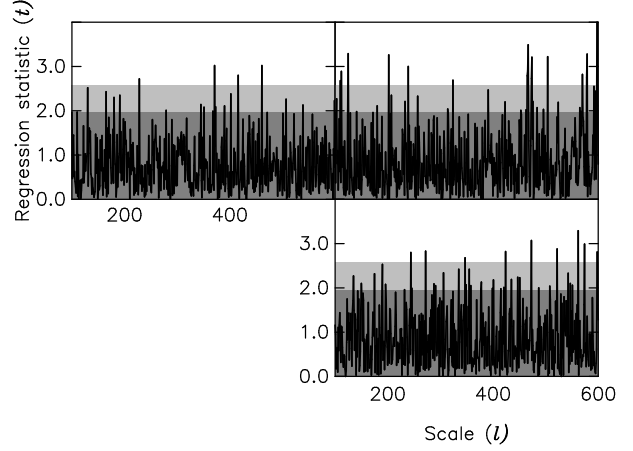


Figure 24. Linear regression results from the $a_{\ell m}$ of the 2 CMB-only maps and a Gaussian MC map.

also the case when we looked at the real space temperature pairs. To illustrate this, we display in Figure 24 the results from the addition of the z_j^2 non-linear term .

6.3 Other results

In light of the positive detections of non-normality, it is obviously important to gain some insight into its cause. In the Introduction, we stated that the distributions resulting from the various sources of non-Gaussianity are poorly understood. Nevertheless, we can reduce the influence of possible contaminants. In particular, by applying a more severe mask to the data we should be able to observe regions of the CMB-sky where there is less Galactic contamination. We looked at the assembly data with the more severe kp0 mask applied. Our techniques produce identical results to those obtained from the kp2 mask: the skewness is consistent with normality; the kurtosis is inconsistent (~ 3.2); D’Agostino’s statistic is inconsistent (ranging from 0.280 to 0.281); and the bivariate kurtosis is inconsistent (~ 8.5). This suggests that Galactic effects may not be causing the non-normality we measure. However, we should be wary of jumping to the conclusion that the signal is cosmological in origin. Over subtraction, residual inhomogeneous noise, or other systematic effects may be the problem.

Another pertinent question is whether the detected non-normality is associated with previous claims of non-Gaussianity. Eriksen et al. (2004) find an asymmetry between the northern and southern Galactic hemispheres, with the northern portion appearing devoid of large-scale structure. Our techniques in real space allow us to localize regions of the sky. We apply our statistic to the northern and southern parts of the *W1* assembly map. We find that the kurtosis, D’Agostino’s and bivariate kurtosis statistics show identical signs of non-normality on both hemispheres. This suggests that the non-normality is symmetric about the Galactic plane. Moreover, this also rules out the non-normality being associated with a localised ‘cold-spot’ as detected by wavelet techniques (McEwen et al. 2005; Vielva et al. 2004).

7 CONCLUSION

In this paper, we have outlined a series of statistics that can be used to assess the multivariate Gaussian nature of CMB data. The extraction of cosmological parameters from this data relies on it being jointly normal. The statistics we describe test differing aspects of joint-normality. The first four statistics assess the normality of marginal distributions using familiar univariate methods. We then utilise three statistics that directly assess joint-normality. Finally, we look for evidence of non-linearity in the relationship between variates. We applied these tests to bivariates extracted from maps derived from the WMAP 1st year data. The maps consisted of 5 frequency maps, 8 'foreground-cleaned' assembly maps and 2 CMB-only maps. The maps were assessed with the kp2 mask applied. The bivariates extracted were temperature pairs (ΔT_1 , ΔT_2) and the real and imaginary parts of the spherical harmonic coefficients $a_{\ell m}$. Although, the latter was only assessed for the two CMB-only maps.

Significant departures from normality were found in all the maps in both real and harmonic spaces. In particular, temperature pairs extracted from all 8 assembly maps were found to be inconsistent with joint-normality. These maps are used to calculate the angular power spectrum and subsequently deduce cosmological parameters. Marginal distributions were found to have values of kurtosis and D'Agostino's statistic outside the 99% confidence regions. Temperatures pairs from the same maps were also found to have values of bivariate kurtosis outside the 99% confidence region. These departures were found at all angular separations. In trying to ascertain the origin of this non-normality, we found that the results were unaffected by the size of the Galactic cut and were evident on either hemisphere of the CMB-sky. This last aspect rules out the non-Gaussianity being related to previous claims of north-south asymmetry or 'cold-spots' detected by wavelet techniques, although residual systematics from the map-making process remain a likely possibility for the origin of the signal.

The transformation techniques for assessing normality described in this paper are quite challenging to implement. In future work, we hope to improve our method such that greater confidence can be placed on the results. One of the benefits of the transformation techniques is that they provide a natural solution to how to modify the data such that it is Gaussian. The positive detections of non-normality seen in bivariate data, should make it worthwhile to assess quantities with larger values of p . This will enable us to build a broader picture of the shape of the distribution. Such knowledge should be supplemented with advances in the understanding of distributions from known sources of non-Gaussianity (whether cosmic or Galactic). The techniques outlined can also be used to study other quantities derived from the data that should conform to joint-normality. For example, the techniques could be applied to coefficients from wavelet or multipole vector analyses. Finally, we note that the techniques can be incorporated into methods for subtracting sources of non-Gaussianity. Firm requirements on the final data, such that they satisfy these tests, will result in cleaner data-sets.

We stress that the currently-available data sets are preliminary; the foreground subtraction for the final CMB-only maps is not perfect, and there may well be residual system-

atics in the instrument noise. Just as the data set is preliminary so is this analysis. We look forward to further releases in order to establish whether the non-Gaussianity that we have detected can be entirely explained by such artifacts.

ACKNOWLEDGEMENTS

We gratefully acknowledge the use of the HEALPix package and the Legacy Archive for Microwave Background Data Analysis (LAMBDA). Support for LAMBDA is provided by the NASA Office of Space Science. This work was supported by PPARC.

REFERENCES

- Adler R. J., 1981, *The Geometry of Random Fields*, Wiley, Chichester.
- Albrecht A. & Steinhardt P., 1982, *Phys. Rev. Lett.*, 48, 1220
- Bardeen J. M., Bond J. R., Kaiser N. & Szalay A. S., 1986.
- Bennett et al., 2003, *ApJS*, 148, 1
- Bennett et al., 2003, *ApJS*, 148, 97
- Box G.E.P. & Cox D.R., 1964, *J. R. Statist. Soc.*, B 26, 211
- Chiang L.-Y., Naselsky P., Verkhodanov, O. & Way, M., 2003, 590, L65
- Chiang L.-Y. & Naselsky P., 2004, preprint (astro-ph/0407395)
- Coles P., Dineen P., Earl J. & Wright D., 2004, *MNRAS*, 350, 983
- Colley W.N., Gott J.R., 2003, *MNRAS*, 344, 686
- Copi C., Huterer D., Starkman G., 2004, *Phys. Rev. D*, 70, 043515
- Cox D.R., Small N.J.H., 1978, *Biometrika*, 65, 263
- D'Agostino R.B., 1971, *Biometrika*, 58, 341
- de Oliveira-Costa A., Tegmark M., Zaldarriaga Z. & Hamilton A., 2004, *Phys. Rev. D*, 69, 063516
- Dineen P. & Coles P., 2004, *MNRAS*, 347, 52
- Efstathiou G., 2003, *MNRAS*, 346, L26
- Efstathiou G., 2004, *MNRAS*, 348, 885
- Eriksen H., Hansen F., Banday A., Gorski K. & Lilje P., 2004, *ApJ*, 605, 14
- Gnanadesikan R., 1997, *Methods for Statistical Data Analysis of Multivariate Observations* – 2nd ed., John Wiley & Sons, New York
- Górski K.M., Hivon E. & Wandelt B.D., 1999, in *Proceedings of the MPA/ESO Conference Evolution of Large-Scale Structure*, eds. A.J. Banday, R.S. Sheth and L. Da Costa, *Partners Ipskamp*, NL, pp. 37-42 (also astro-ph/9812350)
- Guth A., 1981, *Phys. Rev. D*, 23, 347
- Guth A., Pi S.-Y., 1982, *Phys. Rev. Lett.*, 49, 1110
- Hawking S., 1982, *Physics Letters B*, 115, 295
- Hinshaw et al. 2003, *ApJS*, 148, 135
- Land K. & Magueijo J., 2005, 357, 994
- Land K. & Magueijo J., 2005, *Phys. Rev. Lett.*, 95, 071301
- Larson D.L., Wandelt B.D., 2004, *ApJ*, 613, L85
- Linde A., 1982, *Physics Letters B*, 108, 389
- Kibble T., 1976, *J. Phys.*, A9, 1387
- Komatsu E. et al., 2003, *ApJS*, 148, 119
- Krzyszowski W.J., 2000, *Principles of Multivariate Analysis* – Revised ed., Oxford University Press, Oxford
- Mardia K.V., 1970, *Biometrika*, 57, 519
- Mardia K.V., 1980, in *Handbook of Statistics 1*, ed. P.R. Krishnaiah, North-Holland, Amsterdam, pp. 279-320
- McEwen J., Hobson M., Lasenby A. & Mortlock D., 2005, *MNRAS*, 359, 1583
- Medeiros J. & Contaldi C., 2005, preprint (astro-ph/0510816)
- Montgomery D.C., 1997, *Design and Analysis of Experiments* – 4th ed., John Wiley & Sons, New York

- Naselsky P., Doroshkevich A. & Verkhodanov O., 2003, *ApJ*, 599, L53
- Park C.-G., 2004, *MNRAS*, 349, 313
- Press W., Flannery B., Teukolsky S. & Vetterling W., 1992, *Numerical Recipes in C: The Art of Scientific Computing* – 2nd ed., Cambridge University Press, Cambridge
- Stannard A. & Coles P., 2005, *MNRAS*, 364, 929
- Starobinsky A., 1982, *Physics Letters B*, 117, 175
- Tegmark M., de Oliveira-Costa A. & Hamilton A., 2003, *Phys.Rev. D*, 68, 123523
- Vielva P., Martinez-Gonzalez E., Barreiro R., Sanz J & Cayon L., 2004, *ApJ*, 609, 22
- Vilenkin A. & Shellard E., 1994, *Cosmic strings and other topological defects*, Cambridge University Press, Cambridge